Title

Light nuclei collectivity from s NN = 3 GeV Au+Au collisions at RHIC

Authors

Collaboration, STAR
Abdallah, MS
Aboona, BE
et al.

Publication Date

2022-04-01

DOI

10.1016/j.physletb.2022.136941

Physics Letters B 827 (2022) 136941

Contents lists available at ScienceDirect

Physics Letters B

www.elsevier.com/locate/physletb

Light nuclei collectivity from $\sqrt{s_{NN}} = 3$ GeV Au+Au collisions at RHIC

STAR Collaboration

M.S. Abdallah [e], B.E. Aboona [bd], J. Adam [f], L. Adamczyk [b], J.R. Adams [an], J.K. Adkins [ae], G. Agakishiev [ac], I. Aggarwal [ap], M.M. Aggarwal [ap], Z. Ahammed [bj], A. Aitbaev [ac], I. Alekseev [c,aj], D.M. Anderson [bd], A. Aparin [ac], E.C. Aschenauer [f], M.U. Ashraf [l], F.G. Atetalla [ad], G.S. Averichev [ac], V. Bairathi [bb], W. Baker [k], J.G. Ball Cap [u], K. Barish [k], A. Behera [ba], R. Bellwied [u], P. Bhagat [ab], A. Bhasin [ab], J. Bielcik [o], J. Bielcikova [am], I.G. Bordyuzhin [c], J.D. Brandenburg [f], A.V. Brandin [aj], X.Z. Cai [ay], H. Caines [bm], M. Calderón de la Barca Sánchez [i], D. Cebra [i], I. Chakaberia [af], P. Chaloupka [o], B.K. Chan [j], F.-H. Chang [al], Z. Chang [f], A. Chatterjee [l], S. Chattopadhyay [bj], D. Chen [k], J. Chen [ax], J.H. Chen [s], X. Chen [aw], Z. Chen [ax], J. Cheng [bf], S. Choudhury [s], W. Christie [f], X. Chu [f], H.J. Crawford [h], M. Csanád [q], M. Daugherity [a], T.G. Dedovich [ac], I.M. Deppner [t], A.A. Derevschikov [ar], A. Dhamija [ap], L. Di Carlo [bl], L. Didenko [f], P. Dixit [w], X. Dong [af], J.L. Drachenberg [a], E. Duckworth [ad], J.C. Dunlop [f], J. Engelage [h], G. Eppley [at], S. Esumi [bg], O. Evdokimov [m], A. Ewigleben [ag], O. Eyser [f], R. Fatemi [ae], F.M. Fawzi [e], S. Fazio [g], C.J. Feng [al], Y. Feng [as], E. Finch [az], Y. Fisyak [f], A. Francisco [bm], C. Fu [l], C.A. Gagliardi [bd], T. Galatyuk [p], F. Geurts [at], N. Ghimire [bc], A. Gibson [bi], K. Gopal [x], X. Gou [ax], D. Grosnick [bi], A. Gupta [ab], W. Guryn [f], A. Hamed [e], Y. Han [at], S. Harabasz [p], M.D. Harasty [i], J.W. Harris [bm], H. Harrison [ae], S. He [l], W. He [s], X.H. He [aa,*], Y. He [ax], S. Heppelmann [i], S. Heppelmann [aq], N. Herrmann [t], E. Hoffman [u], L. Holub [o], C. Hu [aa], Q. Hu [aa], Y. Hu [s], H. Huang [al], H.Z. Huang [j], S.L. Huang [ba], T. Huang [al], X. Huang [bf], Y. Huang [bf], T.J. Humanic [an], D. Isenhower [a], M. Isshiki [bg], W.W. Jacobs [z], C. Jena [x], A. Jentsch [f], Y. Ji [af], J. Jia [f,ba], K. Jiang [aw], X. Ju [aw], E.G. Judd [h], S. Kabana [bb], M.L. Kabir [k], S. Kagamaster [ag], D. Kalinkin [f,z], K. Kang [bf], D. Kapukchyan [k], K. Kauder [f], H.W. Ke [f], D. Keane [ad], A. Kechechyan [ac], M. Kelsey [bl], Y.V. Khyzhniak [aj], D.P. Kikoła [bk], B. Kimelman [i], D. Kincses [q], I. Kisel [r], A. Kiselev [f], A.G. Knospe [ag], H.S. Ko [af], L. Kochenda [aj], A. Korobitsin [ac], L.K. Kosarzewski [o], L. Kramarik [o], P. Kravtsov [aj], L. Kumar [ap], S. Kumar [aa], R. Kunnawalkam Elayavalli [bm], J.H. Kwasizur [z], R. Lacey [ba], S. Lan [l], J.M. Landgraf [f], J. Lauret [f], A. Lebedev [f], R. Lednicky [ac], J.H. Lee [f], Y.H. Leung [af], N. Lewis [f], C. Li [ax], C. Li [aw], W. Li [at], X. Li [aw], Y. Li [bf], X. Liang [k], Y. Liang [ad], R. Licenik [am], T. Lin [ax], Y. Lin [l], M.A. Lisa [an], F. Liu [l], H. Liu [z], H. Liu [l], P. Liu [ba], T. Liu [bm], X. Liu [an], Y. Liu [bd], Z. Liu [aw], T. Ljubicic [f], W.J. Llope [bl], R.S. Longacre [f], E. Loyd [k], T. Lu [aa], N.S. Lukow [bc], X.F. Luo [l], L. Ma [s], R. Ma [f], Y.G. Ma [s], N. Magdy [m], D. Mallick [ak], S.L. Manukhov [ac], S. Margetis [ad], C. Markert [be], H.S. Matis [af], J.A. Mazer [au], N.G. Minaev [ar], S. Mioduszewski [bd], B. Mohanty [ak], M.M. Mondal [ba], I. Mooney [bl], D.A. Morozov [ar], A. Mukherjee [q], M. Nagy [q], J.D. Nam [bc], Md. Nasim [w], K. Nayak [l], D. Neff [j], J.M. Nelson [h], D.B. Nemes [bm], M. Nie [ax], G. Nigmatkulov [aj], T. Niida [bg], R. Nishitani [bg], L.V. Nogach [ar],

* Corresponding author.
E-mail address: star-publication@bnl.gov (X.H. He).
† Deceased.

https://doi.org/10.1016/j.physletb.2022.136941

T. Nonaka [bg], A.S. Nunes [f], G. Odyniec [af], A. Ogawa [f], S. Oh [af], V.A. Okorokov [aj], K. Okubo [bg], B.S. Page [f], R. Pak [f], J. Pan [bd], A. Pandav [ak], A.K. Pandey [bg], Y. Panebratsev [ac], P. Parfenov [aj], A. Paul [k], B. Pawlik [ao], D. Pawlowska [bk], C. Perkins [h], L.S. Pinsky [u], J. Pluta [bk], B.R. Pokhrel [bc], J. Porter [af], M. Posik [bc], V. Prozorova [o], N.K. Pruthi [ap], M. Przybycien [b], J. Putschke [bl], H. Qiu [aa], A. Quintero [bc], C. Racz [k], S.K. Radhakrishnan [ad], N. Raha [bl], R.L. Ray [be], R. Reed [ag], H.G. Ritter [af], M. Robotkova [am], O.V. Rogachevskiy [ac], J.L. Romero [i], D. Roy [au], L. Ruan [f], A.K. Sahoo [w], N.R. Sahoo [ax], H. Sako [bg], S. Salur [au], E. Samigullin [c], J. Sandweiss [bm,†], S. Sato [bg], W.B. Schmidke [f], N. Schmitz [ah], B.R. Schweid [ba], F. Seck [p], J. Seger [n], R. Seto [k], P. Seyboth [ah], N. Shah [y], E. Shahaliev [ac], P.V. Shanmuganathan [f], M. Shao [aw], T. Shao [s], R. Sharma [x], A.I. Sheikh [ad], D.Y. Shen [s], S.S. Shi [l], Y. Shi [ax], Q.Y. Shou [s], E.P. Sichtermann [af], R. Sikora [b], J. Singh [ap], S. Singha [aa], P. Sinha [x], M.J. Skoby [as], N. Smirnov [bm], Y. Söhngen [t], W. Solyst [z], Y. Song [bm], H.M. Spinka [d,†], B. Srivastava [as], T.D.S. Stanislaus [bi], M. Stefaniak [bk], D.J. Stewart [bm], M. Strikhanov [aj], B. Stringfellow [as], A.A.P. Suaide [av], M. Sumbera [am], B. Summa [aq], X.M. Sun [l], X. Sun [m], Y. Sun [aw], Y. Sun [v], B. Surrow [bc], D.N. Svirida [c], Z.W. Sweger [i], P. Szymanski [bk], A.H. Tang [f], Z. Tang [aw], A. Taranenko [aj], T. Tarnowsky [ai], J.H. Thomas [af], A.R. Timmins [u], D. Tlusty [n], T. Todoroki [bg], M. Tokarev [ac], C.A. Tomkiel [ag], S. Trentalange [j], R.E. Tribble [bd], P. Tribedy [f], S.K. Tripathy [q], T. Truhlar [o], B.A. Trzeciak [o], O.D. Tsai [j], Z. Tu [f], T. Ullrich [f], D.G. Underwood [d,bi], I. Upsal [at], G. Van Buren [f], J. Vanek [am], A.N. Vasiliev [aj,ar], I. Vassiliev [r], V. Verkest [bl], F. Videbæk [f], S. Vokal [ac], S.A. Voloshin [bl], F. Wang [as], G. Wang [j], J.S. Wang [v], P. Wang [aw], X. Wang [ax], Y. Wang [l], Y. Wang [bf], Z. Wang [ax], J.C. Webb [f], P.C. Weidenkaff [t], G.D. Westfall [ai], H. Wieman [af], S.W. Wissink [z], R. Witt [bh], J. Wu [l], J. Wu [aa], Y. Wu [k], B. Xi [ay], Z.G. Xiao [bf], G. Xie [af], W. Xie [as], H. Xu [v], N. Xu [af], Q.H. Xu [ax], Y. Xu [ax], Z. Xu [f], Z. Xu [j], G. Yan [ax], C. Yang [ax], Q. Yang [ax], S. Yang [at], Y. Yang [al], Z. Ye [at], Z. Ye [m], L. Yi [ax], K. Yip [f], Y. Yu [ax], H. Zbroszczyk [bk], W. Zha [aw], C. Zhang [ba], D. Zhang [l], J. Zhang [ax], S. Zhang [m], S. Zhang [s], Y. Zhang [aa], Y. Zhang [aw], Y. Zhang [l], Z.J. Zhang [al], Z. Zhang [f], Z. Zhang [m], F. Zhao [aa], J. Zhao [s], M. Zhao [f], C. Zhou [s], Y. Zhou [l], X. Zhu [bf], M. Zurek [d], M. Zyzak [r]

[a] Abilene Christian University, Abilene, TX 79699
[b] AGH University of Science and Technology, FPACS, Cracow 30-059, Poland
[c] Alikhanov Institute for Theoretical and Experimental Physics NRC "Kurchatov Institute", Moscow 117218, Russia
[d] Argonne National Laboratory, Argonne, IL 60439
[e] American University of Cairo, New Cairo 11835, New Cairo, Egypt
[f] Brookhaven National Laboratory, Upton, NY 11973
[g] University of Calabria & INFN-Cosenza, Italy
[h] University of California, Berkeley, CA 94720
[i] University of California, Davis, CA 95616
[j] University of California, Los Angeles, CA 90095
[k] University of California, Riverside, CA 92521
[l] Central China Normal University, Wuhan, Hubei 430079
[m] University of Illinois at Chicago, Chicago, IL 60607
[n] Creighton University, Omaha, NE 68178
[o] Czech Technical University in Prague, FNSPE, Prague 115 19, Czech Republic
[p] Technische Universität Darmstadt, Darmstadt 64289, Germany
[q] ELTE Eötvös Loránd University, Budapest, H-1117, Hungary
[r] Frankfurt Institute for Advanced Studies FIAS, Frankfurt 60438, Germany
[s] Fudan University, Shanghai, 200433
[t] University of Heidelberg, Heidelberg 69120, Germany
[u] University of Houston, Houston, TX 77204
[v] Huzhou University, Huzhou, Zhejiang 313000
[w] Indian Institute of Science Education and Research (IISER), Berhampur 760010, India
[x] Indian Institute of Science Education and Research (IISER) Tirupati, Tirupati 517507, India
[y] Indian Institute Technology, Patna, Bihar 801106, India
[z] Indiana University, Bloomington, IN 47408
[aa] Institute of Modern Physics, Chinese Academy of Sciences, Lanzhou, Gansu 730000
[ab] University of Jammu, Jammu 180001, India
[ac] Joint Institute for Nuclear Research, Dubna 141 980, Russia
[ad] Kent State University, Kent, OH 44242
[ae] University of Kentucky, Lexington, KY 40506-0055
[af] Lawrence Berkeley National Laboratory, Berkeley, CA 94720
[ag] Lehigh University, Bethlehem, PA 18015
[ah] Max-Planck-Institut für Physik, Munich 80805, Germany
[ai] Michigan State University, East Lansing, MI 48824
[aj] National Research Nuclear University MEPhI, Moscow 115409, Russia
[ak] National Institute of Science Education and Research, HBNI, Jatni 752050, India
[al] National Cheng Kung University, Tainan 70101
[am] Nuclear Physics Institute of the CAS, Rez 250 68, Czech Republic

[an] Ohio State University, Columbus, OH 43210
[ao] Institute of Nuclear Physics PAN, Cracow 31-342, Poland
[ap] Panjab University, Chandigarh 160014, India
[aq] Pennsylvania State University, University Park, PA 16802
[ar] NRC "Kurchatov Institute", Institute of High Energy Physics, Protvino 142281, Russia
[as] Purdue University, West Lafayette, IN 47907
[at] Rice University, Houston, TX 77251
[au] Rutgers University, Piscataway, NJ 08854
[av] Universidade de São Paulo, São Paulo, 05314-970, Brazil
[aw] University of Science and Technology of China, Hefei, Anhui 230026
[ax] Shandong University, Qingdao, Shandong 266237
[ay] Shanghai Institute of Applied Physics, Chinese Academy of Sciences, Shanghai 201800
[az] Southern Connecticut State University, New Haven, CT 06515
[ba] State University of New York, Stony Brook, NY 11794
[bb] Instituto de Alta Investigación, Universidad de Tarapacá, Arica 1000000, Chile
[bc] Temple University, Philadelphia, PA 19122
[bd] Texas A&M University, College Station, TX 77843
[be] University of Texas, Austin, TX 78712
[bf] Tsinghua University, Beijing 100084
[bg] University of Tsukuba, Tsukuba, Ibaraki 305-8571, Japan
[bh] United States Naval Academy, Annapolis, MD 21402
[bi] Valparaiso University, Valparaiso, IN 46383
[bj] Variable Energy Cyclotron Centre, Kolkata 700064, India
[bk] Warsaw University of Technology, Warsaw 00-661, Poland
[bl] Wayne State University, Detroit, MI 48201
[bm] Yale University, New Haven, CT 06520

A R T I C L E I N F O

Article history:
Received 7 December 2021
Received in revised form 24 January 2022
Accepted 28 January 2022
Available online 1 February 2022
Editor: Editor: M. Doser

A B S T R A C T

In high-energy heavy-ion collisions, partonic collectivity is evidenced by the constituent quark number scaling of elliptic flow anisotropy for identified hadrons. A breaking of this scaling and dominance of baryonic interactions is found for identified hadron collective flow measurements in $\sqrt{s_{\mathrm{NN}}}$ = 3 GeV Au+Au collisions. In this paper, we report measurements of the first- and second-order azimuthal anisotropic parameters, v_1 and v_2, of light nuclei (d, t, ^{3}He, ^{4}He) produced in $\sqrt{s_{\mathrm{NN}}}$ = 3 GeV Au+Au collisions at the STAR experiment. An atomic mass number scaling is found in the measured v_1 slopes of light nuclei at mid-rapidity. For the measured v_2 magnitude, a strong rapidity dependence is observed. Unlike v_2 at higher collision energies, the v_2 values at mid-rapidity for all light nuclei are negative and no scaling is observed with the atomic mass number. Calculations by the Jet AA Microscopic Transport Model (JAM), with baryonic mean-field plus nucleon coalescence, are in good agreement with our observations, implying baryonic interactions dominate the collective dynamics in 3 GeV Au+Au collisions at RHIC.

1. Introduction

Collective motion of particle emission in high-energy heavy-ion collisions, often referred to as collective flow, is a general phenomenon observed over a wide range of collision energies. The flow anisotropy parameters, v_n (where n represents the n-th harmonic order), are used to describe the azimuthal anisotropies in particle momentum distributions with respect to the reaction plane [1]. The first- and second-order azimuthal anisotropies, v_1 and v_2, are important probes of nuclear matter. In high energy collisions at the top RHIC and LHC energies, they provide information on the collective hydrodynamic expansion and transport properties of the produced Quark Gluon Plasma (QGP), while at lower collision energies of the order of a few GeV, they are sensitive to the compressibility of the nuclear matter and nuclear equation of state [2,3]. The collision-energy dependence of v_1 and v_2 for different particle species has been observed experimentally [4,5], and provides valuable information on the dynamical evolution of the strongly interacting matter.

At high LHC energies, significant v_2 and v_3 values are reported for d [6,7]. In parallel and at lower energies, compared to protons, enhanced values of v_1 and v_2 for light nuclei (d, t, and ^{3}He) were observed in prior heavy-ion collision experiments [8–14]. These measurements suggest that the v_1 of heavier nuclei have more pronounced energy dependences and may carry more direct information on the collective motion of nuclear matter. Recently, the HADES experiment reported the measurements of anisotropic flow of p, d and t from $\sqrt{s_{\mathrm{NN}}} = 2.4$ GeV Au+Au collisions [15]. The STAR collaboration observed the atomic mass number (A) scaling of light nucleus v_2 for the reduced transverse momentum (p_{T}) range of $p_{\mathrm{T}}/A < 1.5$ GeV/c at $\sqrt{s_{\mathrm{NN}}} = 7.7 - 200$ GeV [14]. Similar to the number of constituent quark (NCQ) scaling of hadron collective flow [16], under the assumptions of small v_n and light nucleus formation by nucleon coalescence in momentum space, light nucleus collective flow is expected to follow an approximate A scaling

$$v_n^A(p_{\mathrm{T}}, y)/A \approx v_n^p(p_{\mathrm{T}}/A, y). \tag{1}$$

The STAR observation [14] favors nucleon coalescence, while the true production mechanism of light nuclei in heavy-ion collisions is still an open question. At lower energies, however, the v_1 is not negligibly small as reported in this paper. Keeping up to v_1^2, Eq. (1) for $n = 2$ becomes

$$v_2^A(p_{\mathrm{T}}, y)/A \approx v_2^p(p_{\mathrm{T}}/A, y) + \frac{A-1}{2}\Big(v_1^p(p_{\mathrm{T}}/A, y)\Big)^2. \tag{2}$$

The coalescence model assumes that light nuclei are formed via the combination of nucleons when these nucleons are near each other both in coordinate and momentum space near the time of kinetic freeze-out [17–20]. Due to the longer passing time of the colliding ions in the few GeV regime, the interference between the expanding central fireball and the spectator remnants becomes more significant than at higher energies. Since flow is strongly affected by the spectators, one expects to gain insight into the collision dynamics and the nucleon coalescence behavior from the measurements of light nucleus v_1 and v_2 in the few GeV energy regime. In this paper, we report the measurements of v_1 and v_2 as functions of particle rapidity (y) and transverse momentum (p_T) for d, t, ^{3}He, and ^{4}He in fixed-target $\sqrt{s_{NN}} = 3$ GeV Au+Au collisions at the STAR experiment.

2. Experiment and data analysis

The data used here were recorded in the fixed-target program by the STAR experiment [21]. The lab energy of the beam is 3.85 GeV per nucleon, equivalent to the center-of-mass energy of $\sqrt{s_{NN}} = 3$ GeV. A detailed description of the STAR detector can be found in [21]. The main tracking and particle identification (PID) detectors are the Time Projection Chamber (TPC) [22] and the Time-of-Flight (TOF) barrel [23] located inside a 0.5 T solenoidal magnetic field. For the fixed target configuration, the Au target is installed inside the vacuum pipe 200 cm to the west of the TPC center. The TPC covers the full azimuth and a pseudorapidity range $0.1 < \eta < 2$, and the TOF covers the range $0.1 < \eta < 1.5$ in the laboratory frame. In this paper, the beam direction is defined as positive, and the particle rapidity is given in the collision center-of-mass frame.

For each event, the reconstructed primary vertex is required to be within 2 cm of the target position along the beam axis. The transverse x, y position of the vertex is required to be within 2 cm of the target located at (0, 2) cm. The event centrality is estimated from the charged-particle multiplicity measured in the TPC within $-2 < \eta < 0$ with the help of a Glauber Monte Carlo model [24].

Charged-track trajectories are reconstructed from the measured space point information in the TPC. In order to select the primary tracks, a requirement of less than 3 cm is applied on their distance of closest approach (DCA) from the event vertex. To avoid effects from track splitting, each track should have at least 15 TPC space points, and have more than 52% of the total possible TPC points used in the track fitting. The TPC reconstruction efficiency is around 80% for all light nuclei species.

The charged particle identification is accomplished by the specific energy loss dE/dx measured in the TPC. Fig. 1a shows the average dE/dx distribution of charged particles as a function of rigidity (momentum/charge). The curves denote the Bichsel expectation for each particle species [25]. At low momenta, the $\langle dE/dx \rangle$ bands corresponding to different particle species are clearly separated and the particle type can be determined via the variable z,

$$z = \ln\left(\frac{\langle dE/dx \rangle}{\langle dE/dx \rangle_B}\right), \tag{3}$$

where the $\langle dE/dx \rangle_B$ is the corresponding Bichsel expectation. The expected value of z for a given particle type is zero. At higher momenta, these bands start to overlap. A combination of z and m^2 of the particle is used to identify the high momentum light nuclei with a PID purity higher than 96%. A particle's m^2, where m is mass of the particle, is determined by measuring the particle speed using the TOF system. Fig. 1b shows the m^2/q^2 distribution as a function of particle rigidity.

The proton v_1 and v_2 are measured over the range of $0.4 < p_T < 2.0$ GeV/c. In this measurement, the lower cutoffs of light nucleus p_T are restricted to the same value in terms of p_T/A (> 0.4 GeV/c). The p_T upper limits are determined based on the

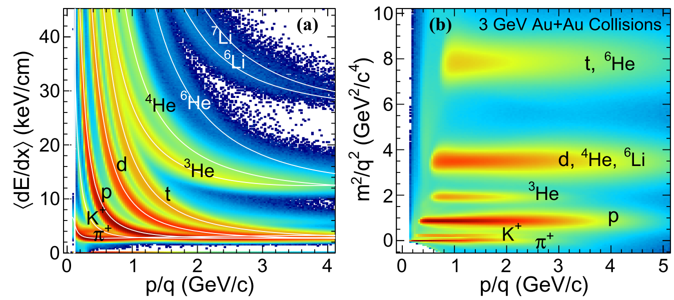

Fig. 1. (a) The $\langle dE/dx \rangle$ of charged tracks versus rigidity in Au+Au collisions at $\sqrt{s_{NN}} = 3$ GeV. The curves are Bichsel expectations for the corresponding particle species as labeled. (b) Particle m^2/q^2 versus rigidity. The bands correspond to π^+, K^+, p, ^{3}He, d, and t as labeled. ^{4}He and ^{6}Li have the same m^2/q^2 as d and ^{6}He has the same m^2/q^2 as t.

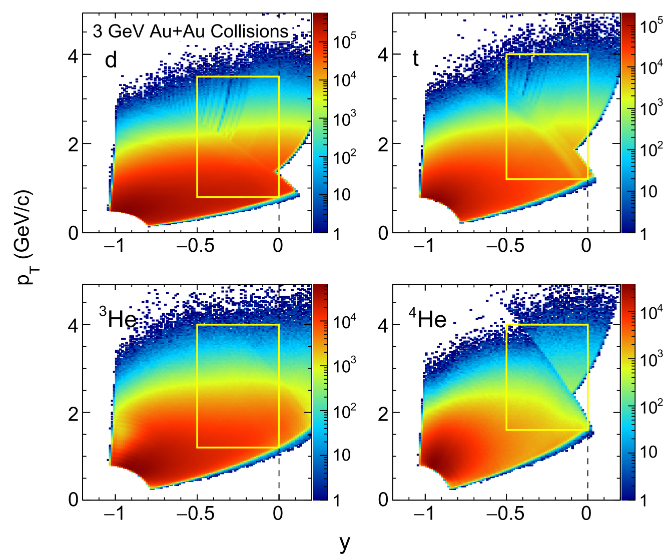

Fig. 2. The p_T versus y acceptances for d, t, ^{3}He, and ^{4}He at $\sqrt{s_{NN}} = 3$ GeV Au+Au collisions. The bands in the distributions are caused by the momentum dependent requirements of the PID. The boxes represent the selected phase space for flow calculation.

p_T versus y acceptances shown in Fig. 2, within $-0.5 < y < 0$ after each studied light nucleus species is identified. The values for v_1 and v_2 are extracted in the chosen p_T ranges: $0.8 < p_T < 3.5$ GeV/c for d, $1.2 < p_T < 4.0$ GeV/c for t and ^{3}He, and $1.6 < p_T < 4.0$ GeV/c for ^{4}He. As a result of the limited η coverage of the TOF detector, within $-0.1 < y < 0$, the t and ^{4}He do not have coverage for $p_T < 2.1$ GeV/c and $p_T < 2.8$ GeV/c, respectively.

The coefficients v_1 and v_2 are determined via a particle's azimuthal angle in momentum space relative to the azimuth of the reaction plane spanned by the beam direction and the impact parameter vector. While the reaction plane orientation can not be accessed directly in measurements, it is common to use the event plane angle to be a proxy of the true reaction plane [1]. In this analysis the first-order event plane Ψ_1 is adopted for both the v_1 and v_2 calculations. The Ψ_1 value is reconstructed by using information from the event plane detector (EPD). A vector

$$\vec{Q} = (Q_x, Q_y) = \left(\sum_i w_i \cos(\phi_i), \sum_i w_i \sin(\phi_i)\right) \tag{4}$$

is calculated event-by-event. The ϕ_i is the azimuthal angle of the i^{th} module of the EPD, and its weight w_i is proportional to the energy deposition. The non-uniformities in the EPD are corrected by subtracting the $(\langle Q_x \rangle, \langle Q_y \rangle)$ from $\vec{Q}$ in each event [1], where

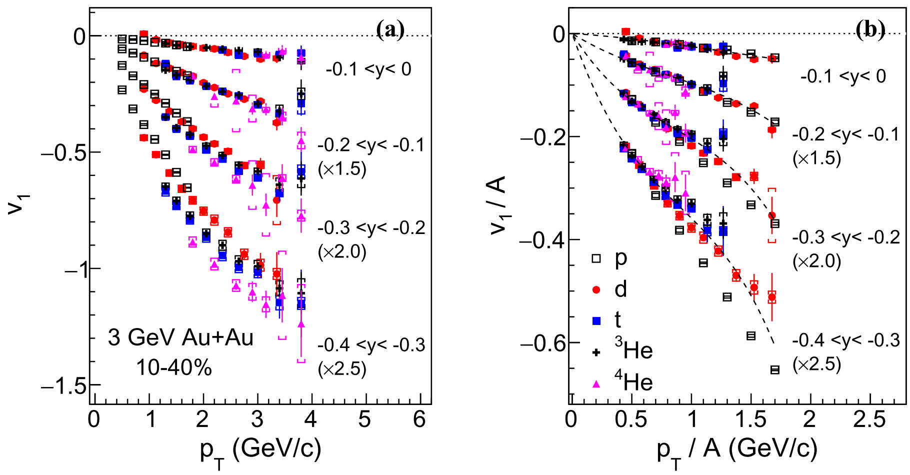

Fig. 3. (a) The p_T and rapidity dependencies of v_1 for p, d, t, ^{3}He, and ^{4}He in 10-40% mid-central Au+Au collisions at $\sqrt{s_{NN}} = 3$ GeV. (b) The same results as (a) but both v_1 and p_T are scaled by A. For t and ^{4}He, there are no data points at $p_T/A < 0.7$ GeV/c in $-0.1 < y < 0$ due to limited acceptance. The data points in each rapidity are scaled for clarity. Statistical and systematic uncertainties are represented by vertical lines and open boxes, respectively. The dashed lines represent the fit to a third-order polynomial function of the data points to guide the eye.

the angle brackets indicate averaging over all events. Then the Ψ_1 is given by $\Psi_1 = \tan^{-1}(Q_y/Q_x)$. A shifting method [1] is utilized to make the distribution of the reconstructed Ψ_1 uniform.

The values v_1 and v_2 are computed via $v_n = \langle\cos[n(\phi - \Psi_1)]\rangle/\mathcal{R}_n$. The p_T- and y-dependent reconstruction efficiency of particle tracks is corrected using a Monte Carlo calculation of simulated particles embedded into real collision events. The event plane resolution $\mathcal{R}_n$ is determined via a three sub-event plane correlation method [1], where the sub-event planes are reconstructed separately in different η ranges of the EPD and TPC. At $\sqrt{s_{NN}} = 3$ GeV, the resolutions peak in the centrality range 30-40% with value of 0.75 and 0.41 for v_1 and v_2, respectively.

The systematic uncertainties of the measured flow harmonics come from the method of selecting charged tracks, from particle identification, and from the event plane resolution. They are estimated point-by-point on v_1 and v_2 as a function of y and p_T for each light nucleus species. The systematic uncertainties arising from the track selection are determined by varying the selection requirements. The values amount to about 2% after the statistical fluctuation effects are removed [26]. The systematic uncertainties related to the particle misidentification are determined by varying the cuts on z and m^2, and are found to be 2% to 8% depending on the light nucleus species and their p_T. A common systematic uncertainty arises from the event plane resolution, and is determined by using combinations of different η sub-events; it is estimated to be less than 2% and 3% for v_1 and v_2, respectively, within the centrality bin 10-40%. Additional systematic uncertainty on the dv_1/dy slope parameter comes from the chosen fit range, and is estimated by taking the difference between the fit values from default range $-0.5 < y < 0$ and from $-0.4 < y < 0$. The typical magnitude of this systematic uncertainty is found to be 3% for all light nucleus species. In the following figures, the total systematic uncertainty of each data point is represented by the open boxes.

3. Results and discussions

The p_T dependencies of the light nucleus v_1 in different rapidity intervals are shown in Fig. 3. Fig. 3b shows that the values of v_1/A of all light nuclei, including protons, approximately follow A scaling for $-0.3 < y < 0$ especially near mid-rapidity. The v_1 scaling behavior suggests the light nuclei are formed via nucleon coalescence in Au+Au collisions at $\sqrt{s_{NN}} = 3$ GeV. The scaling worsens for $p_T/A > 1$ GeV/c in the range $-0.4 < y < -0.3$, where the v_1 values are large and the simple coalescence of Eq. (1) may not apply. Increasing contamination of target-rapidity ($y = -1.045$) fragments may also play a role.

The upper panels of Fig. 4 show the dependencies of v_2 in different rapidity intervals. At mid-rapidity, $-0.1 < y < 0$, the v_2 values are negative for all measured light nucleus species. Moving away from mid-rapidity, the v_2 magnitudes decrease gradually, and become positive for t, ^{3}He, and ^{4}He at larger p_T, while the v_2 of protons and d remain negative within $-0.4 < y < 0$. Moreover, the proton v_2 has a stronger non-monotonic p_T dependence compared to other light nuclei. The lower panels of Fig. 4 show v_2/A as a function of p_T/A and they do not follow the same trend. Taking into account the effect of v_1 by Eq. (2), the naive momentum coalescence expectation of v_2 for d is shown in the dashed curves. While the v_1 effect may partially explain the trend with increasing rapidity, the v_2 data significantly deviate from the curve (shown only for d, but similar behavior is also found for t, ^{3}He, and ^{4}He). This indicates that no A scaling is observed in these data for light nucleus v_2 at $\sqrt{s_{NN}} = 3$ GeV. The A scaling has been observed for $p_T/A < 1.5$ GeV/c in higher energy Au+Au collisions at $\sqrt{s_{NN}} = 7.7 - 200$ GeV [14]. There, as a supporting evidence for the formation of the QGP, the v_2 of hadrons follow an approximate NCQ scaling [27–29].

Fig. 5 shows light nucleus v_1 and v_2 as a function of rapidity integrated in the chosen p_T ranges. There is a clear mass ordering both for v_1 and for v_2, namely, the heavier the mass of a nucleus, the stronger the rapidity dependence in v_1 and v_2. At mid-rapidity, $-0.1 < y < 0$, the value of v_2 is negative and nearly identical for p, d, and ^{3}He. The negative v_2 at mid-rapidity may be caused by shadowing of the spectators as their passage time is comparable with the expansion time of the compressed system at $\sqrt{s_{NN}} = 3$ GeV [11,12]. During the expansion of the participant zone, the particle emission directed toward the reaction plane is blocked by the spectators that are still passing the participant zone. Moving away from mid-rapidity, the proton v_2 remains negative and those of other light nuclei gradually become positive. A similar strong rapidity dependence of light nucleus v_2 has also been reported by the HADES experiment [15]. Nuclear fragmentation may play a role in the production of those light nuclei, the effect of which is beyond the scope of the present investigation.

To further understand light nucleus formation and the scaling behavior of v_1 and v_2, we employ a transport model, Jet AA Microscopic Transportation Model (JAM) [30], to simulate the proton and neutron production from the initial collision stage to the fi-

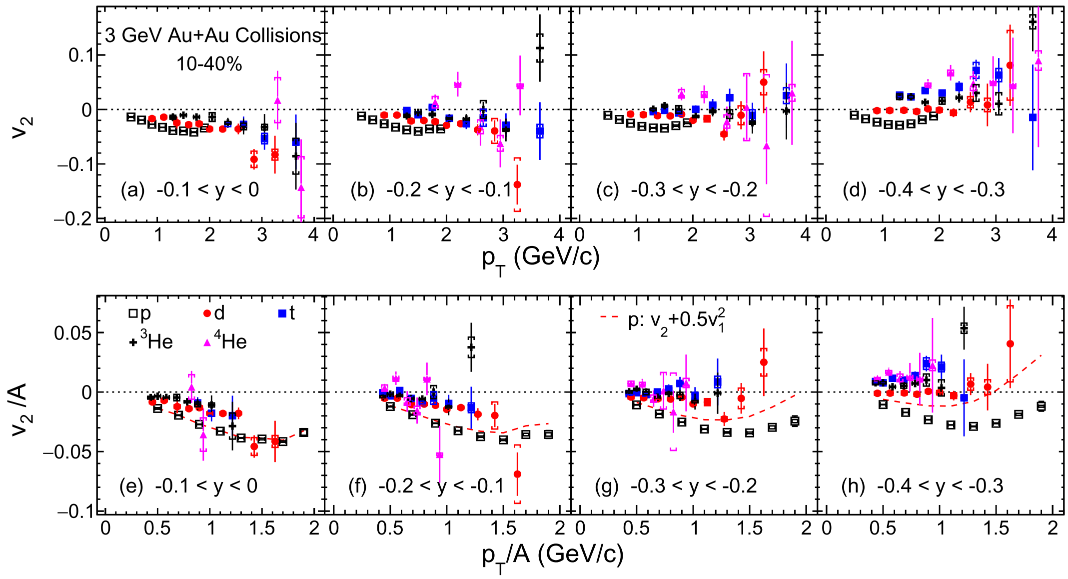

Fig. 4. Upper panels: The p_T and y dependencies of v_2 for p, d, t, ^{3}He, and ^{4}He in 10-40% mid-central Au+Au collisions at $\sqrt{s_{NN}} = 3$ GeV. Lower panels: The same results as in upper panels but both v_2 and p_T are scaled by A. The dashed lines are the v_2 expectation for d by Eq. (2). Statistical and systematic uncertainties are represented by vertical lines and open boxes, respectively.

nal hadron transport in $\sqrt{s_{NN}} = 3$ GeV Au+Au collisions. Both the cascade mode and the mean-field mode of JAM calculations are performed. In the cascade mode, particles are propagated as in vacuum (free streaming) between collisions with other particles. In the mean-field mode [31], a momentum-dependent potential with the incompressibility parameter $\kappa = 380$ MeV is acting on the nucleon evolution. The resulting proton v_1 and v_2 from the mean-field mode are consistent with the experimental observations (see solid-lines in Fig. 5). However, the simulation results from JAM cascade mode underestimate the magnitudes of proton v_1 and give positive values for proton v_2 within $-0.5 < y < 0$, opposite to the data. Note that the calculations from the mean-field mode, which reproduce the observed collectivity of proton and Λ [32], impose stronger repulsive interactions among baryons.

The current JAM model does not create light nuclei. An afterburner, a coalescence approach, is employed to form the light nuclei using the proton and neutron phase-space distributions at a fixed time of 50 fm/c. For each nucleon pair, the momentum and position of each nucleon is boosted to the rest frame of the pair. The relative momentum Δp and the relative coordinate Δr of the two nucleons are evaluated in the rest frame. If the $\Delta p < 0.3$ GeV/c and $\Delta r < 4$ fm, then the nucleon pair is marked as a d [33]. A similar process is used for the formation of t (nnp), ^{3}He (npp) and ^{4}He ($nnpp$), where the constituent nucleons are added one by one according to the Δp and Δr in the rest frame of the nucleon and a light nucleus core. The resulting light nucleus v_1 and v_2, as functions of rapidity, are shown as bands in Fig. 5a and 5b, respectively. Qualitatively both dependencies are well reproduced by the mean-field mode of the JAM plus coalescence calculations. It is noteworthy that the sign change in v_2 of protons (negative) compared to light nuclei (positive) with increasing rapidity is also reproduced by the model calculations. Note, the broken A scaling for light nucleus v_2 is consistent with the nucleon coalescence picture. On the other hand, the cascade mode of the JAM cannot reproduce the measured v_1 and v_2 of protons, as shown by the dash-dotted curves in Fig. 5. As a result, calculations with JAM cascade plus coalescence fail to reproduce the y dependence of v_1 and v_2 of light nuclei.

A first order polynomial function is employed to fit v_1 in Fig. 5a within rapidity range $-0.5 < y < 0$. The extracted slope parameters, dv_1/dy, scaled by A, for light nuclei are shown in Fig. 6 as

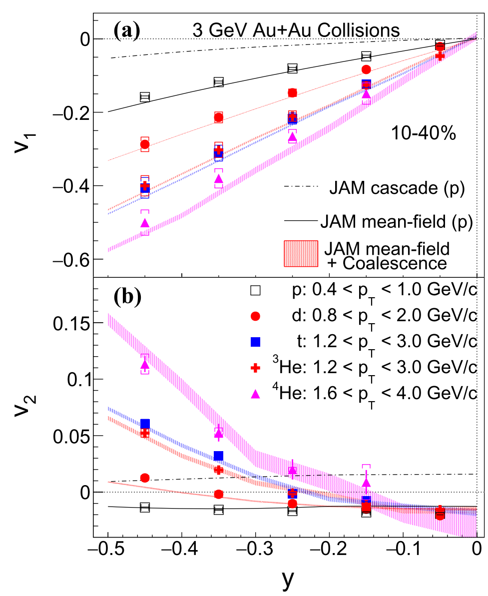

Fig. 5. Rapidity dependencies of light nucleus v_1 (a) and v_2 (b) in 10-40% mid-central Au+Au collisions at $\sqrt{s_{NN}} = 3$ GeV. For t and ^{4}He, the points in $-0.1 < y < 0$ are absent due to limited acceptance. The dash-dotted line and solid line represent the results for protons from the cascade and mean-field modes of JAM, respectively. The bands are the results for light nuclei from JAM mean-field plus coalescence calculations. Systematic uncertainties are represented by open boxes.

functions of the collision energy, together with existing data from higher energies. The values of $(dv_1/dy)/A$ at 3 GeV for all measured light nuclei are positive and grouped together with that of the protons. The results of the JAM model in mean-field mode plus coalescence calculations for p, d, t, ^{3}He and ^{4}He in 3 GeV Au+Au collisions are also shown with corresponding bars. The same experimental cuts have been applied in the calculations and the resulting slope parameters are consistent with the data including the relative order. The agreement between experimental data and model calculations implies that at 3 GeV these light nuclei are formed via the coalescence processes and baryonic interactions dictate their dynamics.

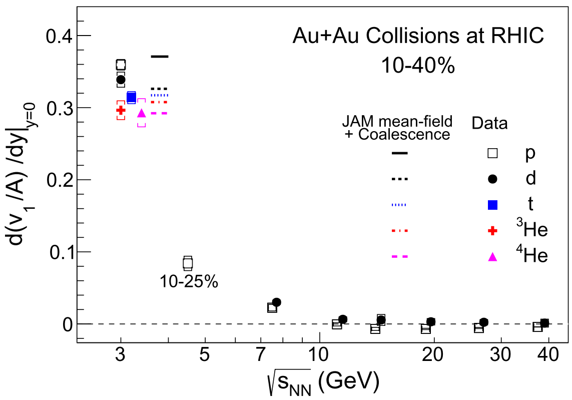

Fig. 6. Light nucleus scaled v_1 slopes $\left(d(v_1/A)/dy|_{y=0}\right)$ as a function of collision energy in 10-40% mid-central Au+Au collisions. Statistical and systematic uncertainties are represented by vertical lines and open boxes, respectively. The data points above 7 GeV are taken from [13]. The proton result at $\sqrt{s_{NN}} = 4.5$ GeV is for 10-25% Au+Au collisions [34]. For clarity, the data points are shifted horizontally. Results of the JAM model in the mean-field mode plus coalescence calculations are shown as color bars.

At higher collision energies, the v_1 of d has been measured from $\sqrt{s_{NN}} = 7.7 - 39$ GeV Au+Au collisions by the STAR experiment [13]. At $\sqrt{s_{NN}} = 7.7$ GeV, the v_1 slope of d follows A scaling within the statistical and systematic uncertainties. For energy $\sqrt{s_{NN}} > 7.7$ GeV, the value of proton dv_1/dy is negative and the corresponding v_1 slopes of d are positive with larger uncertainties. The different scaling behavior of light nuclei dv_1/dy at $\sqrt{s_{NN}} \leq 7.7$ GeV and $\sqrt{s_{NN}} > 11.5$ GeV may indicate a different production mechanism. At higher energies where a QGP is formed, the dominant interactions are partonic in nature. At 3 GeV, baryonic interactions are likely dominant and light nuclei may primarily be formed via coalescence of nucleons. Fragmentation contribution may also play a role which requires further investigation.

4. Summary

In summary, we present the directed flow v_1 and elliptic flow v_2 of d, t, ^{3}He, and ^{4}He for 10-40% centrality in Au+Au collisions at $\sqrt{s_{NN}} = 3$ GeV. The light nucleus v_1, as function of both transverse momentum and particle rapidity, follow an approximate atomic mass number A scaling at rapidity $-0.5 < y < 0$, consistent with the nucleon coalescence model calculations. On the other hand, the light nucleus v_2 do not follow the simple A scaling, even after taking into account the contribution from the comparable magnitude of v_1^2. At mid-rapidity $-0.1 < y < 0$, the value of v_2 is negative for all light nuclei, implying a shadowing effect due to the longer passage time of the spectators. Away from the mid-rapidity, the values of light nucleus v_2 become positive and the corresponding proton v_2 remains negative. The JAM model, with the baryon mean-field (incompressibility parameter κ = 380 MeV and a momentum dependent potential), and a nucleon coalescence qualitatively reproduce both the v_1 and v_2 as functions of rapidity for all reported light nuclei. On the other hand, the results from the JAM cascade mode plus coalescence fail to describe the data. Our results suggest that the light nuclei are likely formed via the coalescence of nucleons at $\sqrt{s_{NN}} = 3$ GeV Au+Au collisions, where baryonic interactions dominate the collision dynamics.

Declaration of competing interest

The authors declare that they have no known competing financial interests or personal relationships that could have appeared to influence the work reported in this paper.

Acknowledgement

We thank the RHIC Operations Group and RCF at BNL, the NERSC Center at LBNL, and the Open Science Grid consortium for providing resources and support. This work was supported in part by the Office of Nuclear Physics within the U.S. DOE Office of Science, the U.S. National Science Foundation, the Ministry of Education and Science of the Russian Federation, National Natural Science Foundation of China, Chinese Academy of Science, the Ministry of Science and Technology of China and the Chinese Ministry of Education, the Higher Education Sprout Project by Ministry of Education at NCKU, the National Research Foundation of Korea, Czech Science Foundation and Ministry of Education, Youth and Sports of the Czech Republic, Hungarian National Research, Development and Innovation Office, New National Excellency Programme of the Hungarian Ministry of Human Capacities, Department of Atomic Energy and Department of Science and Technology of the Government of India, the National Science Centre of Poland, the Ministry of Science, Education and Sports of the Republic of Croatia, ROSATOM of Russia and German Bundesministerium für Bildung, Wissenschaft, Forschung und Technologie (BMBF), Helmholtz Association, Ministry of Education, Culture, Sports, Science and Technology (MEXT) and Japan Society for the Promotion of Science (JSPS).

References

[1] A.M. Poskanzer, S.A. Voloshin, Phys. Rev. C 58 (1998) 1671.
[2] U. Heinz, R. Snellings, Annu. Rev. Nucl. Part. Sci. 63 (2013) 123–151.
[3] P. Danielewicz, R. Lacey, W. Lynch, Science 298 (2002) 1592–1596.
[4] L. Adamczyk, et al., STAR Collaboration, Phys. Rev. Lett. 112 (2014) 162301.
[5] K. Aamodt, et al., ALICE Collaboration, Phys. Rev. Lett. 105 (2010) 252302.
[6] S. Acharya, et al., ALICE Collaboration, Phys. Rev. C 102 (2020) 055203.
[7] S. Acharya, et al., ALICE Collaboration, Eur. Phys. J. C 77 (2017) 658.
[8] M.D. Partlan, et al., EOS Collaboration, Phys. Rev. Lett. 75 (1995) 2100.
[9] S. Wang, et al., EOS Collaboration, Phys. Rev. Lett. 74 (1995) 2646.
[10] J. Barrette, et al., E877 Collaboration, Phys. Rev. C 59 (1999) 884.
[11] G. Stoicea, et al., FOPI Collaboration, Phys. Rev. Lett. 92 (2004) 072303.
[12] W. Reisdorf, et al., FOPI Collaboration, Nucl. Phys. A 876 (2012) 1.
[13] J. Adam, et al., STAR Collaboration, Phys. Rev. C 102 (2020) 044906.
[14] L. Adamczyk, et al., STAR Collaboration, Phys. Rev. C 94 (2016) 034908.
[15] J. Adamczewski-Musch, et al., HADES Collaboration, Phys. Rev. Lett. 125 (2020) 262301.
[16] D. Molnár, S.A. Voloshin, Phys. Rev. Lett. 91 (2003) 092301.
[17] S.T. Butler, C.A. Pearson, Phys. Rev. 129 (1963) 836.
[18] H. Sato, K. Yazaki, Phys. Lett. B 98 (1981) 153.
[19] S. Zhang, J.H. Chen, H. Crawford, D. Keane, Y.G. Ma, Z.B. Xu, Phys. Lett. B 684 (2010) 224.
[20] J. Steinheimer, K. Gudima, A. Botvina, I. Mishustin, M. Bleicher, H. Stöcker, Phys. Lett. B 714 (2012) 85.
[21] K.H. Ackermann, et al., Nucl. Instrum. Methods A 499 (2003) 624.
[22] M. Anderson, et al., Nucl. Instrum. Methods A 499 (2003) 659.
[23] W.J. Llope, Nucl. Instrum. Methods A 661 (2012) S110.
[24] R. Ray, M. Daugherity, J. Phys. G 35 (2008) 125106.
[25] H. Bichsel, Nucl. Instrum. Methods A 562 (2006) 154.
[26] R. Barlow, arXiv:hep-ex/0207026, 2002.
[27] J. Adams, et al., STAR Collaboration, Phys. Rev. Lett. 92 (2004) 052302.
[28] X. Dong, S. Esumi, P. Sorensen, N. Xu, Z. Xu, Phys. Lett. B 597 (2004) 328.
[29] J. Adams, et al., STAR Collaboration, Phys. Rev. Lett. 95 (2005) 122301.
[30] Y. Nara, N. Otuka, A. Ohnishi, K. Niita, S. Chiba, Phys. Rev. C 61 (2000) 024901.
[31] M. Isse, A. Ohnishi, N. Otuka, P.K. Sahu, Y. Nara, Phys. Rev. C 72 (2005) 064908.
[32] M.S. Abdallah, et al., STAR Collaboration, arXiv:2108.00908, 2021.
[33] S. Sombun, K. Tomuang, A. Limphirat, P. Hillmann, C. Herold, J. Steinheimer, Y. Yan, M. Bleicher, Phys. Rev. C 99 (2019) 014901.
[34] M.S. Abdallah, et al., STAR Collaboration, Phys. Rev. C 103 (2021) 034908.